CHEMISTRY
A EUROPEAN JOURNAL

DOI: 10.1002/chem.200700744

Stable Pentacoordinate Carbocations: Structure and Bonding

Israel Fernández,*[a] Einar Uggerud,*[b] and Gernot Frenking*[a]

Abstract: We report that only elements more electropositive than carbon (Group 13, 14, and Be) form stable symmetrical $H_nE{-}CH_3{-}EH_n^+$ structures (E = Group 1, 2, 13, or 14 element) with a planar CH_3 group symmetrically bonded to two EH_n moieties, in analogy with prototypical S_N2 transition structures. Analysis of the bonding situation of these pentacoordinate carbon molecules was studied by means of an energy decomposition analysis (EDA) of the interaction energy. This shows that $H_nE{-}CH_3{-}EH_n^+$ molecules can be viewed as being composed of one CH_3 group that is σ-covalently bonded to two EH_n groups forming a three-center, two-electron bond.

Keywords: bond theory · carbocations · energy decomposition · hypervalent compounds · quantum chemistry

Introduction

The properties of hypervalent compounds have attracted considerable attention during the last few years.[1] In particular, the synthesis and characterization of stable pentacoordinate carbon compounds still constitutes a challenge for this emerging area of interest.[2] Such compounds may either be classified as electron-deficient or electron-rich, based on the number of formal valence electrons around the central carbon. In the former class, the carbon atom has formally eight electrons and the pentacoordinate structure is realized by an interaction between a σ bond (two-center, two-electron bond: 2c–2e) and a vacant orbital of the atom/group linked to the carbon atom. The methonium ion (CH_5^+), carboranes, and a carbon atom in a metal cluster cage belong to this kind of compounds. In contrast, the latter class is characterized by comprising ten electrons around the carbon atom, resulting from an interaction between the vacant 2p orbital of the central carbon with the two lone electron pairs belonging to the nucleophile and the leaving group, respectively. This axial three-center, four-electron E–C–E bond arrangement is normally unstable, in the sense that the pentacoordinate geometry corresponds to a transition structure rather than a minimum. Under special circumstances it is, however, possible to stabilize it, and compounds **1** and **2**, which have been newly isolated by Yamamoto and co-workers are representative examples.[2,3]

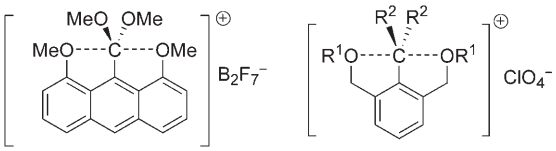

1 **2**

Very recently, Yáñez and co-workers reported the presence of the D_{3h}-symmetric molecule ion **3** as a gas-phase ion–molecule reaction product of tetramethylsilane by using Fourier transform ion cyclotron resonance (FT-ICR) mass spectrometry (Scheme 1).[4] This compound can be viewed

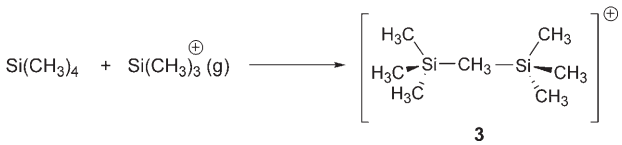

3

Scheme 1.

[a] Dr. I. Fernández, Prof. G. Frenking
Fachbereich Chemie, Philipps-Universität Marburg
Hans-Meerwein-Strasse, 35032 Marburg (Germany)
E-mail: israel@quim.ucm.es
frenking@chemie.uni-marburg.de

[b] Prof. E. Uggerud
Senter for teoretisk og beregningsorientert kjemi
Kjemisk institutt, Universitetet i Oslo
Postboks 1033 Blindern, 0315 Oslo (Norway)
E-mail: einar.uggerud@kjemi.uio.no

Supporting information for this article is available on the WWW under http://www.chemeurj.org/ or from the author: Cartesian coordinates (in Å) and total energies (in a.u.) of all the stationary points discussed in the text.

as a CH_3^+ cation interacting with two $Si(CH_3)_3$ radicals. The model implies that the empty p orbital of the sp^2-hybridized carbon atom interacts with the appropriate singly occupied orbitals of the two $Si(CH_3)_3$ moieties so that the central carbon atom is covalently bonded to the silicon atoms through a three-center, two-electron bond. The proposed D_{3h} species is compatible with the experimentally observed scrambling of the methyl groups and quantum chemical calculations.

We want to point out the resemblance between the above mentioned 3c–2e pentacoordinate carbocation and the prototypical 3c–4e S_N2 transition state structure.[5] Thus, compound **3** corresponds to a condition in which the introduction of electropositive "nucleophile" and "nucleofuge", both being the $SiMe_3$ radical, alters the topography of the potential energy surface (PES). However, such PES topographies are quite common for P, S, or Si, which are well known to form stable pentacoordinate compounds.[6]

The finding by Yáñez et al. prompted us to systematically look for other stable pentacoordinate carbocations analogous to **3** along the periodic table and to investigate their stability limits. In this paper, we report the results of an extensive computational study of the structure and bonding situation of stable pentacoordinate carbocations. In this connection, we need to mention that Jemmis et al.[7] performed HF/STO3-G* calculations of some species of this kind already in 1979.

Computational Details

Complete geometry optimizations were carried out by using DFT and ab initio methods with the GAUSSIAN 03 suite of programs[8] at the B3LYP[9] and MP2[10] levels of theory. We employed the def2/TZVPP triple-ξ quality basis set, which is suggested to be close to the DFT basis-set limit.[11] The vibrational frequencies of the optimized structures were calculated to investigate the nature of the stationary points. The Hessian matrices of the optimized geometries have only positive eigenvalues for the minima on the potential energy surface, whereas transition states present one negative eigenvalue.[12] Atomic partial charges were calculated by using the natural bond orbital (NBO) method.[13]

The bonding analysis of the different species was carried out by using the energy decomposition analysis (EDA) method[14] using the ADF 2006.01 program.[15] In this case, the geometries of the molecules were re-optimized by using the OPBE functional.[16] Uncontracted Slater-type orbitals (STOs) were employed as basis functions for the self-consistent field (SCF) calculations.[17] The basis sets are of triple-ζ quality and are augmented by two sets of polarization functions, that is, p and d functions for the hydrogen atoms and d and f functions for the other atoms. This level of theory is denoted as OPBE/TZ2P. An auxiliary set of s, p, d, f, and g STOs has been employed to fit the molecular densities and to represent the Coulomb and exchange potentials accurately.[18] Scalar relativistic effects were accounted for in the form of the zero-order regular approximation (ZORA).[19]

The interactions were analyzed by means of the energy decomposition analysis (EDA) of the Amsterdam Density Functional program (ADF), which was developed by Ziegler and Rauk[20] following a similar procedure suggested by Morokuma.[21] EDA has proven to give important information about the nature of the bonding in main-group compounds and transition-metal complexes.[14b,22] The focus of the bonding analysis is the instantaneous interaction energy, ΔE_{int}, of the bond, which is the energy difference between the molecule and the fragments in the electronic reference state and frozen geometry of the compound. The interaction energy can be divided into three main components [Eq. (1)]:

$$\Delta E_{int} = \Delta E_{elstat} + \Delta E_{Pauli} + \Delta E_{orb} \quad (1)$$

ΔE_{elstat} gives the electrostatic interaction energy between the fragments, and is calculated by using the frozen electron-density distribution of the fragments in the geometry of the molecules. ΔE_{Pauli} refers to the repulsive interactions between the fragments, which are caused by the fact that two electrons with the same spin cannot occupy the same region in space. ΔE_{Pauli} is calculated by enforcing the Kohn–Sham determinant on the superimposed fragments to obey the Pauli principle by antisymmetrization and renormalization. The stabilizing orbital interaction term, ΔE_{orb}, is calculated in the final step of the energy partitioning analysis when the Kohn–Sham orbitals relax to their optimal form. This term can be further partitioned into contributions by the orbitals belonging to different irreducible representations of the point group of the interacting system. The interaction energy, ΔE_{int}, can be used to calculate the bond-dissociation energy, D_e, by adding ΔE_{prep}, which is the energy necessary to promote the fragments from their equilibrium geometry to the geometry in the compounds [Eq. (2)]:

$$-D_e = \Delta E_{prep} + \Delta E_{int} \quad (2)$$

The advantage of using ΔE_{int} instead of D_e is that the instantaneous electronic interaction of the fragments becomes analyzed, which yields a direct estimate of the energy components. Further details of the energy-partitioning analysis can be found in the literature.[14,23]

Results and Discussion

The aim of the present study is to explore the limits of E atoms along the periodic table that are able to stabilize the CH_3 unit forming hypervalent carbocations. To do this, we calculated the cationic compounds **4–7** that are analogues of **3**. We divide our discussion into five sections, one for each of the Groups 14, 13, 2, and 1, and one concluding one, which includes stability considerations.

PENTACOORDINATE CARBON

4, E= Group 14 element, n = 3
5, E= Group 13 element, n = 2
6, E= Group 2 element, n = 1
7, E= Group 1 element, n = 0

Group 14 cations: The calculations, both with B3LYP/def2-TZVPP and MP2/def2-TZVPP, show that pentacoordinate carbon compounds analogous to the parent compound **3** exist as stable minimum-energy structures for all elements from silicon to lead. Like compounds **3**, the homologues **4-Si**, **4-Ge**, **4-Sn**, and **4-Pb**[24] all have D_{3h} structures with a planar CH_3 group symmetrically bonded to two eclipsed EH_3 moieties. Moreover, the calculated value for the C–Si bond lengths of **4-Si** (2.039 Å) at the MP2/def2-TZVPP level is close to the reported MP2/6–311+G(3df,2pd) value of 2.063 Å for compound **3**.[4] We note that the methyl substitution at silicon in **3** is the only structural difference between the two compounds. In contrast, all efforts to locate a

symmetrical minimum-energy structure for compounds with E=C were fruitless. As expected, **4-C** adopts a typical non-classical geometry in which the methyl and ethyl moieties are bridged by a hydrogen atom (Figure 1). Interestingly, the computed atomic NBO charges in **4-Si** to **4-Pb** show that the positive charge is localized at the EH_3 terminal groups. Although the CH_3 group has a negative charge between -0.28 e and -0.32 e, the EH_n groups carry significant positive charges whose values are $\approx +0.65$ e.

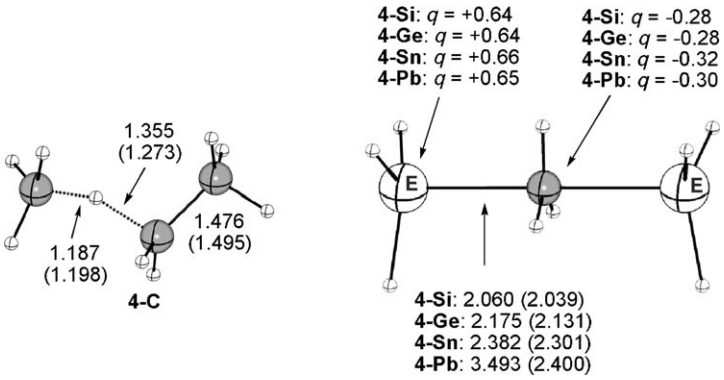

Figure 1. Graphical display of compounds **4-C** to **4-Pb**. All structures correspond to fully optimized geometries. Bond lengths [Å] computed at the B3LYP/def2-TZVPP (plain text) and the MP2/def2-TZVPP (in parenthesis) levels of theory. NBO atomic charges with hydrogen atoms summed into heavy atoms computed at the B3LYP/def2-TZVPP level. Unless otherwise stated, white and gray colors denote hydrogen and carbon atoms, respectively.

To clarify the bonding situation, we re-optimized the geometry of the cations **4-Si** to **4-Pb** at the OPBE/TZ2P level. This method has been recommended to model S_N2 reactions, which involve a pentacoordinate carbon in their transition structures.[25] We then carried out an energy decomposition analysis (EDA) of the interaction between the CH_3 and two EH_3 moieties. Based on the NBO charges in Figure 1, we found it reasonable to consider the decomposition into a $CH_3^{\bullet}$ radical and two "half radical cations" $EH_3^{1/2(+\bullet)}$. The EDA data gathered in Table 1 shows that the interaction energy between the above fragments decreases monotonically as one progresses down the group. From this consideration we also see that the degree of covalent bonding, which is given by the ΔE_{orb} term, is the main contribution to the total attraction. In fact, ΔE_{orb} contributes to 63–70% of the bonding whereas the electrostatic term ΔE_{elstat} only accounts for 30–37%. Interestingly, the splitting of the orbital term into contributions by the orbitals belonging to different irreducible representations of the point group shows that σ bonding contributes to approximately 95–97% whereas the π bonding is almost negligible. Therefore, we can safely conclude that the Group 14 elements containing cations **4-Si** to **4-Pb** are species that posses a pentacoordinate carbon atom σ-covalently bonded to two EH_3 groups (Table 1).

Group 13 cations: We located the C_2-minima **5** with D_{3h} local symmetry at the carbon atom for all members of the group, with the notable exception of **5-Tl**, which adopts a geometry with local C_{3v} symmetry at the carbon atom and two non-equivalent C–Tl bonds (Figure 2). With this exception, the structure of the cationic species **5-B** to **5-In** corresponds to a planar CH_3 group that is symmetrically bonded to two non-eclipsed EH_2 moieties. The computed atomic NBO charges in **5-B** to **5-Tl** show that the positive charge is again localized at the terminal groups. The methyl groups bear a negative charge of between -0.08 e in **5-B** and -0.52 e in **5-Tl**, and the EH_2 groups carry high positive charges ranging from $+0.54$ e in **5-B** to $+0.77$ e in **5-Tl**. The more-positive charges at the terminal groups in compounds **5** relative to compounds **4** are in good agreement with the higher electropositive character of Group 13 elements. However, the differences are small and with this data at hand it is not surprising that we find similar bonding patterns for **5** and **4**. As we will see below, this is also reflected in the EDA.

To distinguish between σ- and π-orbital contributions to the orbital interactions with the EDA method, we reoptimized the geometries of cations **5** with enforced C_s-symmetry constrain by using the MP2 value of the C–E bond length. The energy difference between the C_s structures and the corresponding minima is for all structures <2 kcal mol^{-1} and, therefore, the EDA data of the C_s structures should provide a valid picture of the bonding situation for all compounds **5**. Moreover, because the MP2 geometry of **5-Tl** has nearly identical C–Tl bond lengths, we decided to include the latter compound in the EDA study by using the shorter MP2 value of the C–Tl interatomic distance (2.431 Å) for both bonds. As readily seen from Table 2, the interaction energy between the methyl radical and two EH_2 fragments

Table 1. Results of the energy decomposition analysis at the OPBE/TZ2P level for cations **4-Si** to **4-Pb**. Energy values in kcal mol^{-1}.

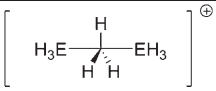

E	Si	Ge	Sn	Pb
ΔE_{int}	−96.6	−81.6	−70.6	−58.6
ΔE_{Pauli}	243.0	214.7	187.0	139.8
ΔE_{elstat}[a]	−102.0 (30.0%)	−95.6 (32.2%)	−86.6 (33.6%)	−73.9 (37.3%)
ΔE_{Orb}[a]	−273.7 (70.0%)	−200.8 (67.8%)	−171.1 (66.4%)	−124.4 (62.7%)
ΔE_{σ}[b]	−225.1 (94.7%)	−192.3 (95.8%)	−165.2 (96.5%)	−120.0 (96.5%)
ΔE_{π}[b]	−12.6 (5.3%)	−8.5 (4.2%)	−5.9 (3.5%)	−4.4 (3.5%)
r(C–E) [Å]	2.058	2.165	2.367	2.469
fragments	H_3E (1/2 e, $q=+0.5$), $CH_3^{\bullet}$ (d), EH_3 (1/2 e, $q=+0.5$)			

[a] The percentage values in parentheses give the contribution to the total attractive interactions $\Delta E_{elstat}+\Delta E_{orb}$. [b] The percentage values in parentheses give the contribution to the total orbital interactions ΔE_{orb}.

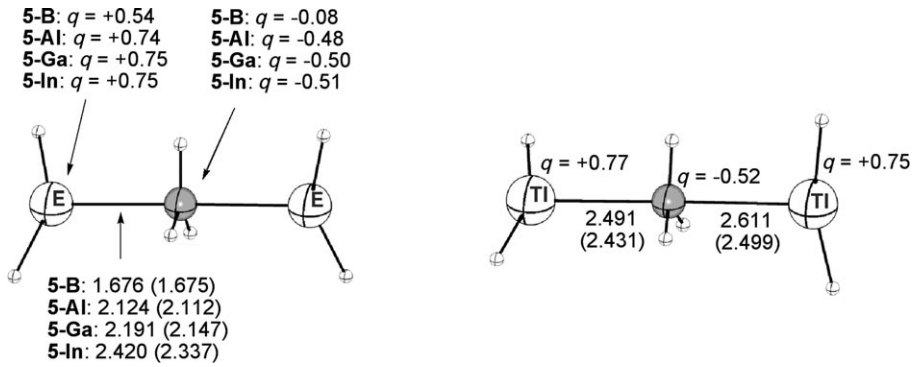

Figure 2. Graphical display of compounds **5-B** to **5-Tl**. All structures correspond to fully optimized geometries. Bond lengths [Å] computed at the B3LYP/def2-TZVPP (plain text) and the MP2/def2-TZVPP (in parenthesis) levels of theory. NBO atomic charges with hydrogen atoms summed into heavy atoms computed at the B3LYP/def2-TZVPP level. See Figure 1 legend for additional details.

Table 2. Results of the energy decomposition analysis at the OPBE/TZ2P level for cations **5-B** to **5-Tl**. Energy values in kcal mol^{-1}.

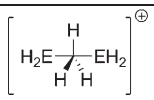

E	B	Al	Ga	In	Tl
ΔE_{int}	−125.8	−91.5	−79.2	−65.3	−53.2
ΔE_{Pauli}	289.0	185.4	191.8	175.0	157.1
ΔE_{elstat}[a]	−134.0 (32.3%)	−101.7 (36.7%)	−108.5 (40.0%)	−100.8 (41.9%)	−85.8 (40.8%)
ΔE_{Orb}[a]	−280.9 (67.7%)	−175.2 (63.3%)	−162.5 (60.0%)	−139.5 (58.1%)	−124.5 (59.2%)
ΔE_{σ}[b]	−268.3 (95.5%)	−171.0 (97.6%)	−158.7 (97.6%)	−136.8 (98.1%)	−122.3 (98.2%)
ΔE_{π}[b]	−12.6 (4.5%)	−4.2 (2.4%)−3.8 (2.4%)	−2.7 (1.9%)	−2.2 (1.8%)	
fragments	H_2E (1/2 e, $q=+0.5$), $CH_3^{\bullet}$ (d), EH_2 (1/2 e, $q=+0.5$)				

[a] The percentage values in parentheses give the contribution to the total attractive interactions $\Delta E_{elstat} + \Delta E_{orb}$. [b] The percentage values in parentheses give the contribution to the total orbital interactions ΔE_{orb}.

decreases monotonically as one progresses from boron to thallium. Again, the main contribution to the total attraction comes from the orbital term ranging from 68% in **5-B** to 59% in **5-Tl**, which is clearly larger than the electrostatic term. Nevertheless, we want to point out that the electrostatic bonding is higher in compounds **5** relative to cations **4**, in good agreement with the higher NBO charges for the Group 13 cations. The partition of the orbital term into the different symmetry contributors also shows that these species are σ bonded (95–98%) while the π bonding is almost negligible. In this respect, we can conclude that there is little difference in the bonding situation between **4** and **5**.

Group 2 cations: The theoretical results for the pentacoordinate carbocations of Group 2 elements **6-E** are significantly different from those of Groups 13 and 14, **4-E** and **5-E**. We could only locate one D_{3h}-symmetrical species, namely **6-Be**. For the rest of the members of Group 2, the D_{3h} species are saddle points of order 1 or higher, ranging from being a transition structure with a weak imaginary mode for magnesium ($i=-89\ cm^{-1}$, B3LYP/def2-TZVPP) to having five imaginary frequencies of vibration for the symmetrical structures between calcium and barium. The energy difference between the D_{3h} structure of **6-Mg**, which is a saddle point, and the corresponding minimum, which has C_{3v} symmetry but similar values for the C–Mg bond lengths, is negligible (<0.1 kcal mol^{-1}). This result is in qualitative agreement with the calculation by von R. Schleyer and co-workers at the HF/STO-3G* level.[7] Therefore, we consider the **6-Mg** cation as a highly fluxional structure, gliding easily between two mirror C_{3v} structures. The cases of **6-Ca** to **6-Ba** are radically different because the minimum structures have clearly non-equivalent C–E bonds with C_{3v}-local symmetry at the central carbon atom (Figure 3). As expected, in the latter species the energy difference between the D_{3h} cations and the corresponding minima is quite large (ranging from 9.6 kcal mol^{-1} in **6-Ca** to 26.0 kcal mol^{-1} in **6-Ba** at the B3LYP/def2-TZVPP level). Moreover, the NBO charges in both minima and transition structures for **6-Be** to **6-Ba** show that the positive charge is strongly built up at the EH groups, leaving the CH_3 group with a negative charge ranging from −0.75 e in **6-Be** to −0.92 e in **6-Ba**. Again, the higher positive values fit well with the more electropositive character of these elements relative to Groups 13 and 14.

Taking the energy differences between the transition state structures and the minima into account, we decided to analyze the bonding situation of cations **6** only for the symmetrical D_{3h} species **6-Be** and **6-Mg** by using a fragmentation scheme similar to that of cations **4** and **5**. From the data in Table 3, we conclude that Group 2 carbocations **6** present a bonding situation similar to that of the related symmetrical compounds **4** and **5**, in which the pentacoordinate carbon atom is σ-covalently bonded to two EH groups forming a 3c–2e bond.

Group 1 cations: No D_{3h}-symmetrical structure was found as a minimum on the potential energy surfaces for any of the elements E = Li–Cs. Inspection of the Hessian matrices of the D_{3h} structures showed that they have one imaginary frequency, which means that they are transition states at the B3LYP and MP2 levels. For Li, our result is at odds with Jemmis et al. who reported that the trigonal-bypyramidal D_{3h} structure of **7-Li** is a minimum on the potential energy

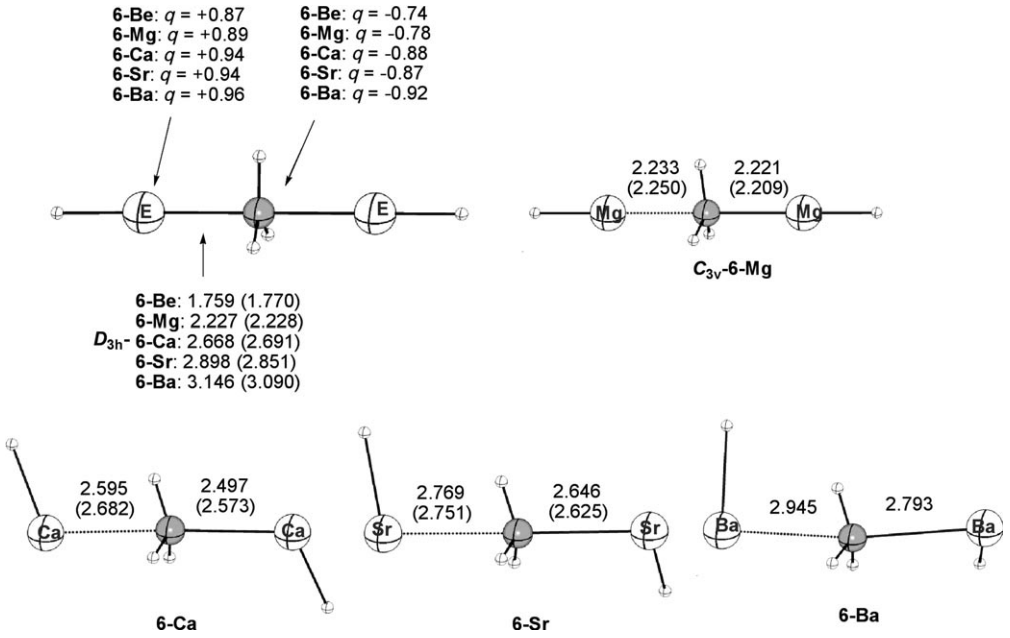

Figure 3. Graphical representations of compounds **6-Be** to **6-Ba**. All structures correspond to fully optimized geometries. Bond lengths [Å] computed at the B3LYP/def2-TZVPP (plain text) and the MP2/def2-TZVPP (in parenthesis) levels of theory. NBO atomic charges with hydrogen atoms summed into heavy atoms computed at the B3LYP/def2-TZVPP level. See Figure 1 legend for additional details.

Table 3. Results of the energy decomposition analysis at the OPBE/TZ2P level for cations **6-Be** and **6-Mg**. Energy values in kcal mol^{-1}.

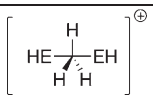

E	Be	Mg
ΔE_{int}	−121.3	−75.8
ΔE_{Pauli}	192.7	119.5
ΔE_{elstat}[a]	−101.8 (32.4%)	−64.6 (33.0%)
ΔE_{Orb}[a]	−212.2 (67.6%)	−130.6 (66.9%)
ΔE_{σ}[b]	−201.6 (95.0%)	−127.9 (97.9%)
ΔE_{π}[b]	−10.6 (5.0%)	−2.7 (2.1%)
r(C–E) [Å]	1.771	2.245
fragments	HE (+1/2), $CH_3^{\bullet}$ (d), EH (+1/2)	

[a] The percentage values in parentheses give the contribution to the total attractive interactions $\Delta E_{elstat}+\Delta E_{orb}$. [b] The percentage values in parentheses give the contribution to the total orbital interactions ΔE_{orb}.

surface at the HF/3–21G level.[7] The difference between their results and our data may be due to the different levels of theory that were employed. We want to point out that a trigonal-bypyramidal pentacoordinate carbon structure was reported on the basis of an X-ray crystallographic analysis for tetrakis(benzylsodium-TMEDA) (TMEDA = tetramethylethylenediamine).[26] This points to an active role of the substituent at the carbon atom in stabilizing the hypervalent structure. The cations **7-Li** to **7-Cs** adopt C_{3v}-minimum geometries with two different C–E bond lengths. Interestingly, the energy difference between the D_{3h} saddle points and the C_{3v} minima is in no case higher than 2.0 kcal mol^{-1}, which indicates the dynamic character of these structures (Figure 4).

Because the energy difference between the C_{3v} and D_{3h} structures is small, we also analyzed the bonding situation of the symmetrical D_{3h} cations **7** by using the same fragmentation scheme used for cations **4**, **5**, and **6** for comparison reasons. From the data in Table 4, we can conclude that Group 1 D_{3h} carbocations **7** present a bonding situation similar to that of the above related symmetrical compounds in which

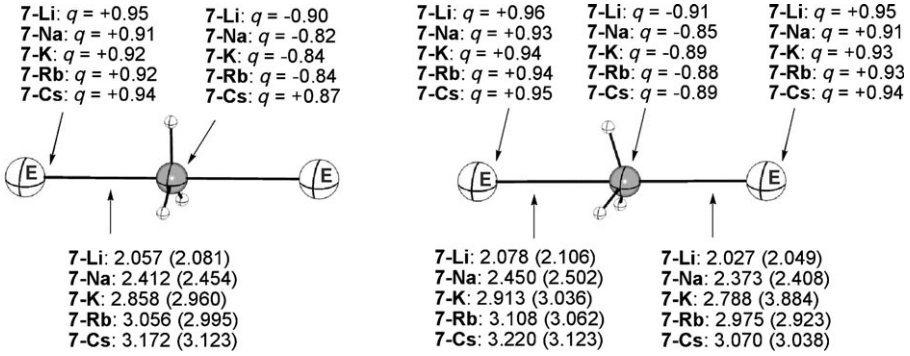

Figure 4. Graphical representations of D_{3h}-transition state structures **7-Li** to **7-Cs** (left) and C_{3v} minima (right). All structures correspond to fully optimized geometries. Bond lengths [Å] computed at the B3LYP/def2-TZVPP (plain text) and the MP2/def2-TZVPP (in parenthesis) levels of theory. NBO atomic charges with hydrogen atoms summed into heavy atoms computed at the B3LYP/def2-TZVPP level. See Figure 1 legend for additional details.

Table 4. Results of the energy decomposition analysis at the OPBE/TZ2P level for the D_{3h} saddle point cations **7-Li** to **7-Cs**. Energy values in kcal mol^{-1}.

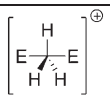

E	Li	Na	K	Rb	Cs
ΔE_{int}	−70.2	−48.3	−42.7	−40.7	−42.1
ΔE_{Pauli}	61.8	40.8	47.5	37.1	42.3
ΔE_{elstat}[a]	−24.2 (18.4%)	−14.8 (16.7%)	−16.1 (17.9%)	−11.1 (14.3%)	−13.3(15.7%)
ΔE_{orb}[a]	−107.7 (81.6%)	−74.2 (83.3%)	−74.1 (82.1%)	−66.8 (85.7%)	−71.2 (84.3%)
ΔE_{σ}[b]	−107.5 (99.7%)	−74.0 (99.7%)	−74.0 (99.9%)	−66.7 (99.9%)	−71.1 (99.9%)
ΔE_{π}[b]	−0.2 (0.3%)	−0.2 (0.3%)	−0.1 (0.1%)	−0.1 (0.1%)	−0.1 (0.1%)
fragments	E (+1/2), $CH_3^{\bullet}$ (d), E (+1/2)				

[a] The percentage values in parentheses give the contribution to the total attractive interactions $\Delta E_{elstat} + \Delta E_{orb}$. [b] The percentage values in parentheses give the contribution to the total orbital interactions ΔE_{orb}.

the pentacoordinate carbon atom is σ-covalently bonded to two E groups forming a 3c–2e bond.

Stability of the symmetrical cations 4–6: The stability of the symmetrical energy-minimum species **4–6** towards dissociation was also addressed. We computed the dissociation energies D_1 to D_4 for the four possible dissociation pathways depicted in Scheme 2 at the MP2/def2-TZVPP level and also

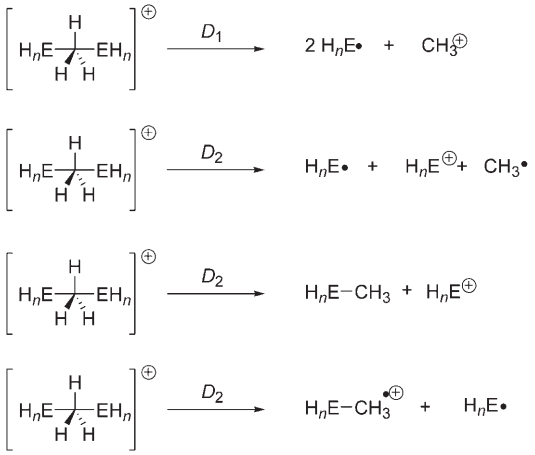

Scheme 2. Dissociation pathways for cations **4–6**.

at the CCSD(T)/def2-TZVPP//MP2-def2-TZVPP level.

From the data collected in Table 5, it is clear that all the considered dissociation processes are highly endothermic, with the D_3 process being the least unfavorable. Interestingly, the computed dissociation energies follow a trend similar to that of the interaction energies obtained from the EDA. Therefore, we can conclude that pentacoordinate carbocations **4–6** are quite stable species in the gas phase. Moreover, the stability of the latter compounds decreases slightly as one progresses from top to bottom and from left to right in the periodic table.

Notably, the symmetrical $H_nE{-}CH_3{-}EH_n^+$ structure is found only for elements more electropositive than carbon. We may consider these cations to be the protonated forms of $H_nE{-}CH_2{-}EH_n$. For elements more electronegative than carbon, it is known that protonation of $H_nE{-}CH_2{-}EH_n$ will preferably take place at the more basic site, which in these cases is the E atom, thereby giving complexes of the type $H_{n+1}E{\cdots}CH_2{-}EH_n^+$.[27] Upon changing to an element with an electronegativity value less than that of carbon, the E–C bond polarity is inverted, and consequently protonation will instead take place at the central C atom. The situation in which $EH_n{=}CH_3$ (propane) is borderline between these extremes is particularly illustrating. The corresponding protonated cation forms a typical non-classical ion structure in which the proton is shared between the central and one of the terminal carbons. For the most electropositive elements, charge transfer from E to C will result in the formation of extremely polar bonds. This becomes an unstable situation, which inevitably leads to spontaneous decomposition, for example, into $Li^+{\cdots}CH_3Li$.

Conclusion

From the computational study reported the following conclusions can be drawn:

1) We predict that symmetrical pentacoordinate carbon-containing cations **4–6** are stable molecules and experimentally accessible, certainly so in the gas phase.

Table 5. Dissociation energies[a] [kcal mol^{-1}] of symmetrical cations **4–6**.

Compound	D_1	D_2	D_3	D_4
4-Si	172.3 (166.0)	131.7 (127.3)	38.1 (36.4)	98.4 (93.5)
4-Ge	164.0 (158.0)	121.4 (116.8)	35.3 (33.7)	90.4 (85.7)
4-Sn	162.7 (156.8)	111.9 (106.7)	34.8 (32.8)	85.7 (80.7)
4-Pb	152.9 (146.3)	99.2 (92.7)	32.1 (29.2)	76.1 (70.3)
5-B	188.8 (184.0)	150.6 (146.9)	40.5 (38.7)	109.9 (105.7)
5-Al	187.7 (182.9)	124.0 (120.6)	37.8 (36.6)	99.6 (95.8)
5-Ga	180.8 (174.8)	113.8 (109.6)	30.7 (29.6)	92.1 (87.6)
5-In	177.0 (170.4)	100.7 (95.6)	27.7 (26.3)	83.0 (77.9)
6-Be	196.7 (193.6)	162.8 (160.5)	68.2 (67.3)	117.4 (114.7)

[a] First value indicates the dissociation energy at the MP2/def2-TZVPP level and the second value (in parenthesis) at the CCSD(T)/def2-TZVPP//MP2/def2-TZVPP level.

2) The structure of the latter species consists of a planar CH_3 group that is symmetrically bonded to two EH_n moieties similar to prototypical S_N2 transition structures. The latter are characterized by being saddle points of the respective reaction potential surfaces. Therefore, the present examples correspond to a condition in which the introduction of electropositive "nucleophiles" and leaving groups, EH_n, alters the topography of the potential energy surface.
3) The bonding analysis of these compounds clearly shows that the $CH_3(EH_n)_2^+$ can be viewed as a central CH_3 fragment that is σ-covalently bonded to two EH_n moieties forming three-center, two-electron bonds.

Acknowledgements

This work was supported by the Deutsche Forschungsgemeinschaft. I. Fernández acknowledges the Ministerio de Educación y Ciencia (Spain) for a postdoctoral fellowship.

[1] a) K.-y. Akiba, *Chemistry of Hypervalent Compounds*, Wiley-VCH, New York, **1999**; b) E. Block, *Heteroatom Chemistry*, VCH, New York, **1990**.
[2] M. Yamashita, Y. Yamamoto, K.-y. Akiba, D. Hashizume, F. Iwasaki, N. Takagi, S. Nagase, *J. Am. Chem. Soc.* **2005**, *127*, 4354, and references therein.
[3] K.-y. Akiba, Y. Moriyama, M. Mizozoe, H. Inohara, T. Nishii, Y. Yamamoto, M. Minoura, D. Hashizume, F. Iwasaki, N. Takagi, K. Ishimura, S. Nagase, *J. Am. Chem. Soc.* **2005**, *127*, 5893.
[4] J. A. Dávalos, R. Herrero, J-L. M. Abboud, O. Mó, M. Yáñez, *Angew. Chem.* **2007**, *119*, 385; *Angew. Chem. Int. Ed.* **2007**, *46*, 381.
[5] E. Uggerud, *Chem. Eur. J.* **2006**, *12*, 1127.
[6] a) T. I. Solling, A. Pross, L. Radom, *Int. J. Mass Spectrom.* **2001**, *210–211*, 1; b) T. I. Solling, L. Radom, *Chem. Eur. J.* **2001**, *7*, 1516; c) M. A. vanBochove, M. M. Swart, F. M. Bickelhaupt, *J. Am. Chem. Soc.* **2006**, *128*, 10738; d) A. P. Bento, F. M. Bickelhaupt, *J. Org. Chem.* **2007**, *72*, 2201.
[7] a) E. D. Jemmis, J. Chandrasekhar, P. von R. Schleyer, *J. Am. Chem. Soc.* **1979**, *101*, 527; b) P. von R. Schleyer, B. Tidor, E. D. Jemmis, J. Chandrasekhar, E.-U. Würthwein, A. J. Kos, B. T. Luke, J. A. Pople, *J. Am. Chem. Soc.* **1983**, *105*, 484.
[8] Gaussian 03, Revision D.01, M. J. Frisch, G. W. Trucks, H. B. Schlegel, G. E. Scuseria, M. A. Robb, J. R. Cheeseman, J. A. Montgomery, Jr., T. Vreven, K. N. Kudin, J. C. Burant, J. M. Millam, S. S. Iyengar, J. Tomasi, V. Barone, B. Mennucci, M. Cossi, G. Scalmani, N. Rega, G. A. Petersson, H. Nakatsuji, M. Hada, M. Ehara, K. Toyota, R. Fukuda, J. Hasegawa, M. Ishida, T. Nakajima, Y. Honda, O. Kitao, H. Nakai, M. Klene, X. Li, J. E. Knox, H. P. Hratchian, J. B. Cross, V. Bakken, C. Adamo, J. Jaramillo, R. Gomperts, R. E. Stratmann, O. Yazyev, A. J. Austin, R. Cammi, C. Pomelli, J. W. Ochterski, P. Y. Ayala, K. Morokuma, G. A. Voth, P. Salvador, J. J. Dannenberg, V. G. Zakrzewski, S. Dapprich, A. D. Daniels, M. C. Strain, O. Farkas, D. K. Malick, A. D. Rabuck, K. Raghavachari, J. B. Foresman, J. V. Ortiz, Q. Cui, A. G. Baboul, S. Clifford, J. Cioslowski, B. B. Stefanov, G. Liu, A. Liashenko, P. Piskorz, I. Komaromi, R. L. Martin, D. J. Fox, T. Keith, M. A. Al-Laham, C. Y. Peng, A. Nanayakkara, M. Challacombe, P. M. W. Gill, B. Johnson, W. Chen, M. W. Wong, C. Gonzalez, and J. A. Pople, Gaussian, Inc., Wallingford CT, **2004**.
[9] a) A. D. Becke, *J. Chem. Phys.* **1993**, *98*, 5648; b) C. Lee, W. Yang, R. G. Parr, *Phys. Rev. B* **1998**, *37*, 785.
[10] a) J. S. Binkley, J. A. Pople, *Int. J. Quantum Chem.* **1975**, *9*, 229; b) J. A. Pople, J. S. Binkley, R. Seeger, *Int. J. Quantum Chem. Symp.* **1976**, *10*, 1.
[11] F. Weigend, R. Alhrichs, *Phys. Chem. Chem. Phys.* **2005**, *7*, 3297.
[12] J. W. McIver, A. K. Komornicki, *J. Am. Chem. Soc.* **1972**, *94*, 2625.
[13] a) J. P. Foster, F. Weinhold, *J. Am. Chem. Soc.* **1980**, *102*, 7211; b) A. E. Reed, F. J. Weinhold, *J. Chem. Phys.* **1985**, *83*, 1736; c) A. E. Reed, R. B. Weinstock, F. Weinhold, *J. Chem. Phys.* **1985**, *83*, 735; d) A. E. Reed, L. A. Curtiss, F. Weinhold, *Chem. Rev.* **1988**, *88*, 899.
[14] Recent reviews about the EDA method and its application have been published by: a) F. M. Bickelhaupt, E. J. Baerends, *Rev. Comput. Chem.* **2000**, *15*, 1; b) M. Lein, G. Frenking, *Theory and Applications of Computational Chemistry: The First 40 Years* (Eds.: C. E. Dykstra, G. Frenking, K. S. Kim, G. E. Scuseria), Elsevier, Amsterdam, 291 (**2005**).
[15] G. te Velde, F. M. Bickelhaupt, E. J. Baerends, S. J. A. van Gisbergen, C. Fonseca Guerra, J. G. Snijders, T. Ziegler, *J. Comput. Chem.* **2001**, *22*, 931.
[16] a) N. C. Handy, A. Cohen, *J. Mol. Phys.* **2001**, *99*, 403; b) J. P. Perdew, K. Burke, M. Ernzerhof, *Phys. Rev. Lett.* **1996**, *77*, 3865.
[17] J. G. Snijders, E. J. Baerends, P. Vernooijs, *At. Nucl. Data Tables* **1982**, *26*, 483.
[18] J. Krijn, E. J. Baerends, *Fit Functions in the HFSMethod*, Internal Report (in Dutch), Vrije Universiteit Amsterdam, The Netherlands, **1984**.
[19] a) C. Chang, M. Pelissier, P. Durand, *Phys. Scr.* **1986**, *34*, 394; b) J.-L. Heully, I. Lindgren, E. Lindroth, S. Lundquist, . A.-M. Martensson-Pendrill, *J. Phys. B* **1986**, *19*, 2799; c) E. van Lenthe, E. J. Baerends, J. G. Snijders, *J. Chem. Phys.* **1993**, *99*, 4597; d) E. van Lenthe, E. J. Baerends, J. G. Snijders, *J. Chem. Phys.* **1996**, *105*, 6505; e) E. van Lenthe, R. van Leeuwen, E. J. Baerends, J. G. Snijders, *Int. J. Quantum Chem.* **1996**, *57*, 281.
[20] T. Ziegler, A. Rauk, *Theor. Chim. Acta* **1977**, *46*, 1.
[21] K. Morokuma, *J. Chem. Phys.* **1971**, *55*, 1236.
[22] a) G. Frenking, K. Wichmann, N. Fröhlich, C. Loschen, M. Lein, J. Frunzke, V. M. Rayón, *Coord. Chem. Rev.* **2003**, *238–239*, 55; b) C. Esterhuysen, G. Frenking, *Theor. Chem. Acc.* **2004**, *111*, 81; c) A. Kovács, C. Esterhuysen, G. Frenking, *Chem. Eur. J.* **2005**, *11*, 1813; d) A. Krapp, F. M. Bickelhaupt, G. Frenking, *Chem. Eur. J.* **2006**, *12*, 9196.
[23] a) F. M. Bickelhaupt, E. J. Baerends in *Reviews in Computational Chemistry, Vol. 15* (Eds.: K. B. Lipkowitz, D. B. Boyd), Wiley-VCH, New York, **2000**, p. 1.
[24] The D_{3h}-symmetrical **4-Pb** cation presents a low-lying imaginary mode ($i = -40\ cm^{-1}$) at the B3LYP level, which disappears at the MP2 and OPBE levels of theory.
[25] M. Swart, M. Solá, F. M. Bickelhaupt, *J. Comput. Chem.* **2007**, *28*, 1551.
[26] C. Schade, P. von R. Schleyer, *J. Am. Chem. Soc.* **1986**, *108*, 2484.
[27] E. Uggerud, *J. Chem. Soc. Perkin Trans. 2* **1996**, 1915.

Received: May 16, 2007
Revised: June 7, 2007
Published online: July 23, 2007

